PNAS RESEARCH ARTICLE | DEVELOPMENTAL BIOLOGY OPEN ACCESS

Dual genetic tracing demonstrates the heterogeneous differentiation and function of neuromesodermal progenitors in vivo

Hengwei Jin[a,1], Zixin Liu[a,1], Jialing Mou[a], Muxue Tang[a], Xiuzhen Huang[a], Kuo Liu[b], Qianyu Zhang[c], Kathy O. Lui[d,2], and Bin Zhou[a,b,c,2]

Affiliations are included on p. 10.

Edited by Marianne Bronner, California Institute of Technology, Pasadena, CA; received February 6, 2024; accepted March 4, 2025

In recent decades, the traditional paradigm of three distinct germ layers formed during gastrulation has been revised with the identification of neuromesodermal progenitors (NMPs). These progenitors emerge during gastrulation and contribute to both the neural ectoderm, particularly the spinal cord, and the adjacent paraxial mesoderm [D. Henrique *et al.*, *Development* 142, 2864–2875 (2015); R. J. Garriock *et al.*, *Development* 142, 1628–1638 (2015); E. Tzouanacou *et al.*, *Dev. Cell* 17, 365–376 (2009)]. However, effective genetic tools for lineage tracing and functional assessments of NMPs in vivo are currently lacking. Here, we developed a dual recombinase–mediated genetic system to specifically trace and ablate Brachyury^{+}Sox2^{+} NMPs. Our genetic tracing and single-cell RNA sequencing analyses revealed that NMPs consist of three distinct unipotent and bipotent progenitor populations that progressively differentiate into neural and mesodermal fates. Genetic depletion of NMPs demonstrated their critical role in trunk and tail formation. This study provides in vivo genetic evidence supporting the heterogeneity of NMPs in terms of cell fate determination and their functional roles in the developing embryo.

neuromesodermal progenitors | Sox2 | brachyury | bi-potent progenitors | dual genetic lineage tracing

Significance

Neuromesodermal progenitors (NMPs) play pivotal roles in embryonic development and hold unique potential in regenerative medicine. Previous studies have used pluripotent stem cell differentiation systems in vitro and single-molecule labeling tracing systems in vivo to investigate NMPs. However, the distribution and stemness of NMPs at a single-cell resolution have yet to be fully determined. In this study, we developed a series of dual recombinase–mediated genetic tools specifically designed for labeling NMPs in vivo. These tools are valuable for studying the cell fate determination and functional roles of NMPs.

During early gastrulation, the pluripotent epiblast produces the surface ectoderm, neuroectoderm, mesoderm, and endoderm (1). As the embryo transitions into the elongation stage, multiple cell populations collaborate to organize the patterning of the trunk and tail. Neuromesodermal progenitors (NMPs) are initially located at the node–streak border (NSB) and the adjacent caudal lateral epiblast (CLE), later migrating to the chordoneural hinge region of the tail bud (2–5). Recent studies have suggested that this cell population can self-renew and contribute to the elongation of both the spinal cord and the adjacent paraxial mesoderm (6–9). NMPs are characterized as a transient population that arises early in gastrulation, expands during the late organogenesis stage, and subsequently decreases along the body axis (6, 10). They are identified by the expression of two key markers: *brachyury (T)*, an early mesodermal marker, and *Sox2,* a neural progenitor marker (6, 11–15). The expression of *T* is regulated by WNT and FGF signaling pathways and serves as an early regulator of trunk and tail development (16, 17). Conversely, *Sox2* is expressed in most neural precursors and is essential for maintaining neural cells in a progenitor state (13, 18). Wnt3a/β-catenin signaling is required for balancing the differentiation potential of bipotent NMPs into mesodermal and neural lineages (7, 8). Additional signaling pathways, such as FGF and BMP (19, 20), also play significant roles in the regulation of NMP specification. The precise coordination of these molecular interactions is essential for proper lineage commitment and segmental body plan in vertebrates.

Based on the rare spontaneous reversion of a lacZ gene to an active lacZ gene, single cells were randomly labeled, and their fate mapping was previously investigated (21). These retrospective clonal lineage analyses suggested that NMPs were bipotent in the elongating mouse embryo (21). However, this method does not directly indicate the precise location of NMPs or the specific time window in which they appear during embryonic development. Although methods for generating NMPs from embryonic stem cells or epiblast stem cells in vitro have been well established (4, 9, 22), there are currently no specific genetic tools available for directly labeling NMPs and tracking their cell fate to examine their differentiation potential in vivo. This gap highlights the need for novel approaches to study NMPs more comprehensively.

Here, we used single-cell RNA sequencing (scRNA-seq) and dual recombinase–mediated genetic lineage tracing to study the contribution of NMPs to somitogenesis in mouse

Author contributions: H.J. and B.Z. designed research; H.J., Z.L., J.M., M.T., X.H., K.L., and Q.Z. performed research; H.J., Z.L., K.O.L., and B.Z. analyzed data; and H.J., K.O.L., and B.Z. wrote the paper.

The authors declare no competing interest.

This article is a PNAS Direct Submission.

[1]H.J. and Z.L. contributed equally to this work.

[2]To whom correspondence may be addressed. Email: kathyolui@cuhk.edu.hk or zhoubin@sibs.ac.cn.

This article contains supporting information online at https://www.pnas.org/lookup/suppl/doi:10.1073/pnas.2402305122/-/DCSupplemental.

Published April 3, 2025.

embryos. Genetic fate mapping revealed that NMPs primarily localize in the caudal region of the embryo at E8.5 and subsequently contribute to differentiated neural and mesodermal tissues. Surprisingly, T^+Sox2^+ cells were also found to generate a subset of endodermal derivatives. Clonal analysis further confirmed the bipotency of NMPs at a single-cell resolution. Functionally, the specific ablation of NMPs resulted in trunk and tail abnormalities, underscoring their crucial role in proper embryonic development.

Results

Single-Cell Transcriptomics Defines the Molecular Markers of NMPs. Specific genetic targeting of endogenous NMPs is critical for understanding their in vivo cell fate and differentiation potential during embryonic development. To date, no single marker can uniquely denote NMPs. However, two molecular markers, the early mesodermal control factor *Brachyury* (*T*) and the key neural progenitor regulator *Sox2*, are commonly used to label NMPs (6, 11–15). To characterize T^+Sox2^+ NMPs in detail, we first performed genome-wide scRNA-seq on murine cells isolated from E8.5 posterior tissues (23) (Fig. 1*A*). After quality control, a total of 15,250 cells were retained for further analysis by Seurat (24). Based on the expression of representative genes determined by unsupervised clustering, the isolated cells were categorized into 14 distinct clusters (Fig. 1 *B* and *C*), which included NMP, neural tube, somite, and presomitic mesoderm (PSM). We then conducted CellChat analysis to explore the relationships between different clusters. Ligands secreted from NMP, PSM, somite, and the neural tube were grouped into an outgoing pattern 2, indicating specific signaling pathways such as Notch, Fgf, and MK pathways (Fig. 1*D*). The receptors expressed in these cell clusters were categorized into an incoming pattern 1, primarily associated with the MK, Notch, BMP, and Wnt signaling pathways (Fig. 1*E*). These results indicated significant intercellular communication among the NMP, PSM, neural tube, and somite clusters. In addition, we found that *Sox2* was predominantly expressed in the NMP and neural tube clusters, while *T* was primarily found in the NMP, PSM, and somite clusters (Fig. 1*F*). Consistent with previous studies (6, 11–15), NMPs were defined by the intersectional activation of *T* and *Sox2* expression (Fig. 1*F*). Furthermore, compared to the other 13 clusters, the gene expression map further showed additional molecular signatures for NMPs, including *Nkx1-2* (8), *Epha5*, *Fgf17*, and *Fgf8* (Fig. 1*G*).

Regarding the potential signaling pathways that drive lineage differentiation, previous studies have reported that the conserved Wnt/FGF/RA and Sox2/T/Tbx6 regulatory networks collaborate to maintain the competence of NMPs in generating multigerm progenitors. Specifically, Wnt and Fgf signaling pathways are required for mesodermal cell fate determination, while BMP signaling promotes NMPs to adopt a mesodermal fate via repressing *Sox2* activation (6, 19, 25). Moreover, TBX6-dependent *Sox2* repression is crucial for the development of paraxial mesoderm derived from NMPs (26, 27). Conversely, RA signaling suppresses Wnt signaling and regulates the differentiation of NMPs into the neural lineage (9, 28). In our scRNA-seq data, we found that as NMPs transitioned into the neural tube, the expression levels of *Sox1* and *Pax6* increased, indicating neural differentiation. In contrast, during the differentiation of NMPs into somites, the expression of *Tbx6*, *Mesp1*, and *Meox1* was noted, which is indicative of mesoderm induction (*SI Appendix*, Fig. S1*A*). Furthermore, our analysis revealed that Wnt signaling, FGF signaling, and the BMP inhibitor *Bambi* gradually decreased, coinciding with an increase in RA signaling and Notch signaling during the bidirectional differentiation of NMPs (*SI Appendix*, Fig. S1*B*). After NMPs differentiated, the expression levels of these genes progressively decreased (*SI Appendix*, Fig. S1*B*).

In order to provide a more comprehensive understanding of the biopotency of NMPs, we integrated scRNA-seq data from publicly available datasets at E7.5 (29), E9.5 (30), and E10.5 (31) with our E8.5 dataset (*SI Appendix*, Fig. S1 *C* and *D*). This analysis revealed that NMPs first appeared as early as E7.5, while radial glia and neurons predominantly emerged after E9.5 (*SI Appendix*, Fig. S1*D*). We found that T^+Sox2^+ cells were primarily localized within the NMP cluster (*SI Appendix*, Fig. S1*E*), consistent with previous findings. To further analyze the data, we employed diffusion map analysis to calculate diffusion pseudotime for each cell. This analysis clearly indicated that NMPs could differentiate into both neural and somite lineages over time (*SI Appendix*, Fig. S1*F*). Focusing on NMPs within the integrated data allowed us to identify two distinct subclusters, designated NMP1 and NMP2 (*SI Appendix*, Fig. S1*G*). NMP1 was predominantly present at E7.5, while NMP2 emerged progressively after E7.5, accompanied by a decline in NMP1, which nearly disappeared by E10.5 (*SI Appendix*, Fig. S1*G* and S1*H*). GO enrichment analysis revealed that NMP2 was upregulated in pathways associated with anterior/posterior pattern specification, skeletal system development, and nervous system development (*SI Appendix*, Fig. S1*I*). These findings underscore the pivotal functions of NMP2 in pattern specification and its dual differentiation potential. We hypothesized that NMP1 may serve as precursors to NMP2, with NMP2 gradually acquiring the capacity for bipotent differentiation into neuronal and somite lineages. Additionally, we observed an upregulation of Hox family genes, including *Hoxc6*, *Hoxc9*, and *Hoxc10*, in NMP2 (*SI Appendix*, Fig. S1*J*). These genes may act as potential drivers, contributing to the establishment of body axis patterns and promoting tissue-specific differentiation. The top 10 genes that were found to be significantly upregulated or downregulated in NMP2 compared to NMP1 are displayed in *SI Appendix*, Fig. S1*J*. Feature plots further illustrated representative upregulated genes (*Gm10260* and *Hoxc10*) and downregulated genes (*Cdx1* and *Wnt8a*) (*SI Appendix*, Fig. S1*K*).

Additionally, when comparing our mouse dataset to published datasets from chick (32) and macaque (33), we observed similar cell types across different species exhibiting spatial proximity in UMAP embeddings, suggesting transcriptional similarities (*SI Appendix*, Fig. S1*L*). However, differential gene expression and enrichment analysis showed that NMP clusters from different species displayed diverse pathway enrichment. In comparison to the macaque dataset, mouse NMPs showed enrichment in BMP signaling, Notch signaling, neurotrophin signaling, and ErbB signaling pathways. In contrast, macaque NMPs were enriched in integrin-mediated signaling, PI3K-Akt signaling, insulin-like growth factor receptor signaling, and transforming growth factor beta receptor signaling pathways. Interestingly, when compared to the chick dataset, mouse NMPs exhibited significantly increased angiogenesis, Wnt signaling, and BMP signaling. Meanwhile, chick NMPs displayed enrichment in Notch signaling, fibroblast growth factor receptor signaling, and TGF-beta signaling pathways (*SI Appendix*, Fig. S1*M*). These findings highlight the evolutionary conservation of NMPs while also emphasizing the distinct regulatory pathways that may contribute to species-specific developmental processes.

Furthermore, we subsetted the T^+Sox2^+ cells at E8.5 and performed PCA based on highly variable genes across these cells. The UMAP analysis of the T^+Sox2^+ cells revealed that they could be categorized into 13 principal components (Fig. 1*H*). Subsequently, we reclustered these T^+Sox2^+ cells and identified eight distinct subpopulations (C1–C8) (Fig. 1*J*). Our analysis indicated that

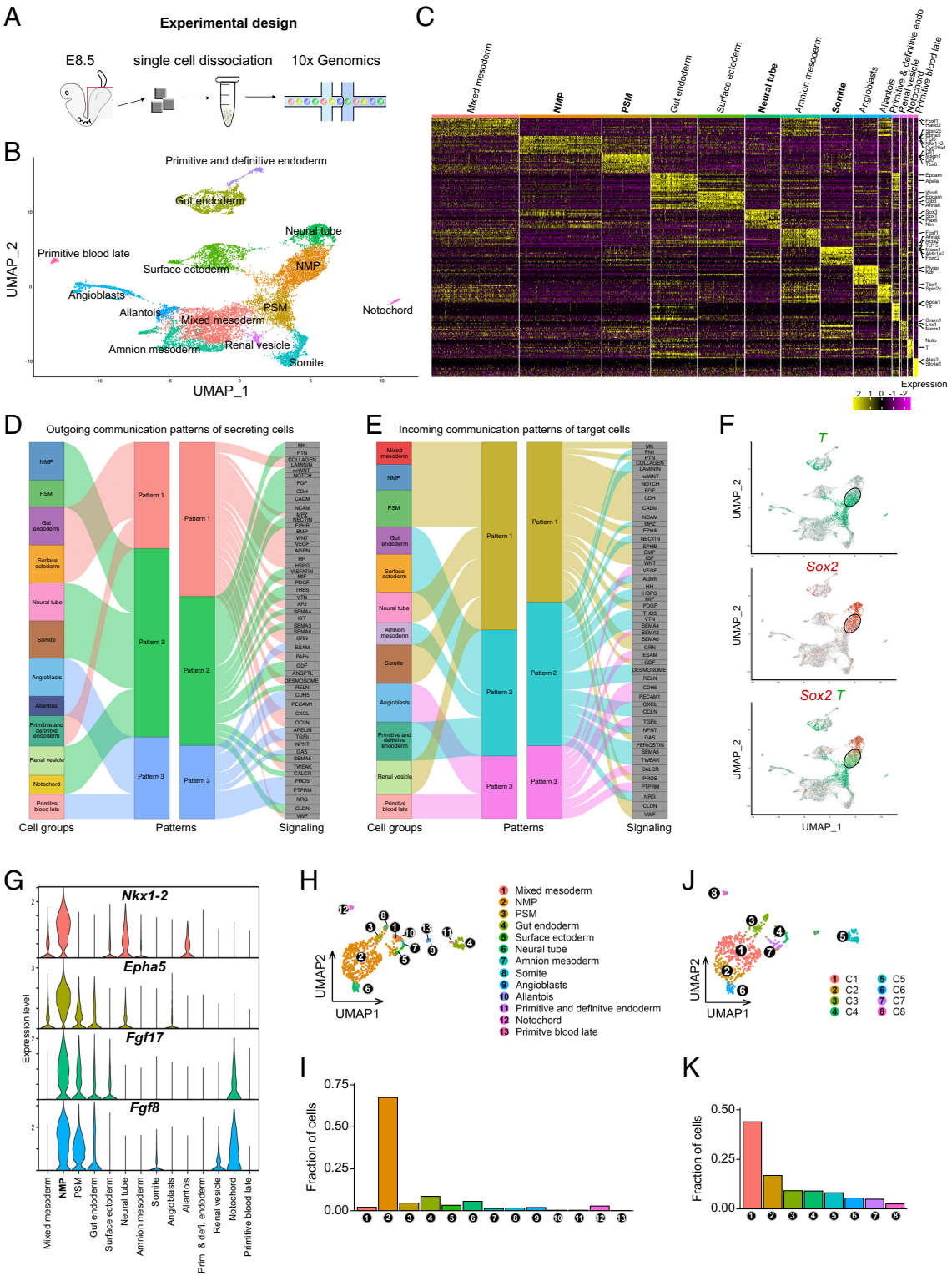

Fig. 1. Characterization of NMPs by scRNA-seq. (*A*) Experimental design for single-cell transcriptional profiling of NMPs dissected from the caudal region of E8.5 mouse embryos. (*B*) Uniform Manifold Approximation and Projection (UMAP) embedding showing 14 clusters of 15,250 single cells. (*C*) Hierarchical clustering of expression heatmaps displaying differentially expressed marker genes of the 14 identified clusters. (*D*) The inferred outgoing communication patterns of secreting cells. The *Left* panel shows the correspondence between the cell groups and inferred latent patterns, while the *Right* panel shows the correspondence between patterns and signaling pathways. The thickness of the flow indicates the contribution of the cell groups or signaling pathway to each latent pattern. (*E*) The inferred incoming communication patterns of target cells. (*F*) UMAP colored by expression of mesodermal and neural markers *T* (green) and *Sox2* (red). (*G*) Violin plots depicting the RNA expression level of potential molecular signature in NMPs. (*H–K*) UMAP embedding of $T^{+}Sox2^{+}$ cells derived from the E8.5 dataset, based on principal component analysis (PCA) performed exclusively on high variable genes (HVGs) of $T^{+}Sox2^{+}$ cells. Panel *H* shows cluster annotations corresponding to the previous E8.5 dataset, while panel *J* presents the reclustering of $T^{+}Sox2^{+}$ cells into 8 subpopulations. Panels *I* (corresponding to *H*) and *K* (corresponding to *J*) depict the proportions of each cluster within the $T^{+}Sox2^{+}$ cell population. NMPs; PSM.

most T^+Sox2^+ cells predominately fell into the NMP clusters (C1 and C2), consistent with the expression patterns characteristic of NMPs (Fig. 1 *I* and *K*). Specifically, we observed higher expression levels of *Nkx1-2* and *Lix1* in the NMP cluster. Additionally, *Cdx4*, *Epha5*, and *Wnt3a* were more specifically expressed in C1, while *Sox3*, *Hes3*, and *Ncam1* were enriched in C2 (*SI Appendix*, Fig. S2 *A* and *B*). Taken together, these scRNA-seq data confirmed that *T* and *Sox2* serve as relatively specific molecular markers of NMPs, suggesting that NMPs possess the potential to differentiate into both neural and somite lineages over time.

Establishing a Dual Genetic Tracing System for Tracing NMPs. Given that the intersectional activation of *T* and *Sox2* specifically marks NMPs, we employed dual orthogonal recombination systems, Cre-*loxP* and Dre-*rox* (34), to genetically label endogenous T^+Sox2^+ NMPs. We designed two distinct genetic strategies for tracing NMPs (Figs. 2 and 3). In the first strategy, we used a Rosa26-traffic light reporter (*R26-TLR*) (35) to simultaneously label 3 populations: T^+, $Sox2^+$, and T^+Sox2^+ cells (Fig. 2*A*). Following tamoxifen (Tam) treatment, *T-DreER* was used to label T^+ cells with ZsGreen, while *Sox2-CreER* labeled $Sox2^+$ cells with tdTomato (tdT). Notably, T^+Sox2^+ cells were marked as $ZsGreen^+tdT^+$ and displayed yellow fluorescence, serving as a readout (Fig. 2 *A* and *B*). This approach allowed us to concurrently trace T^+, $Sox2^+$, and T^+Sox2^+ cells within a single embryo.

To validate this design, we first generated *T-DreER* knock-in mice and crossed them with *R26-TLR* reporter mice (*SI Appendix*, Fig. S3 *A–D*). Following Tam treatment at E7.5, $ZsGreen^+$ cells

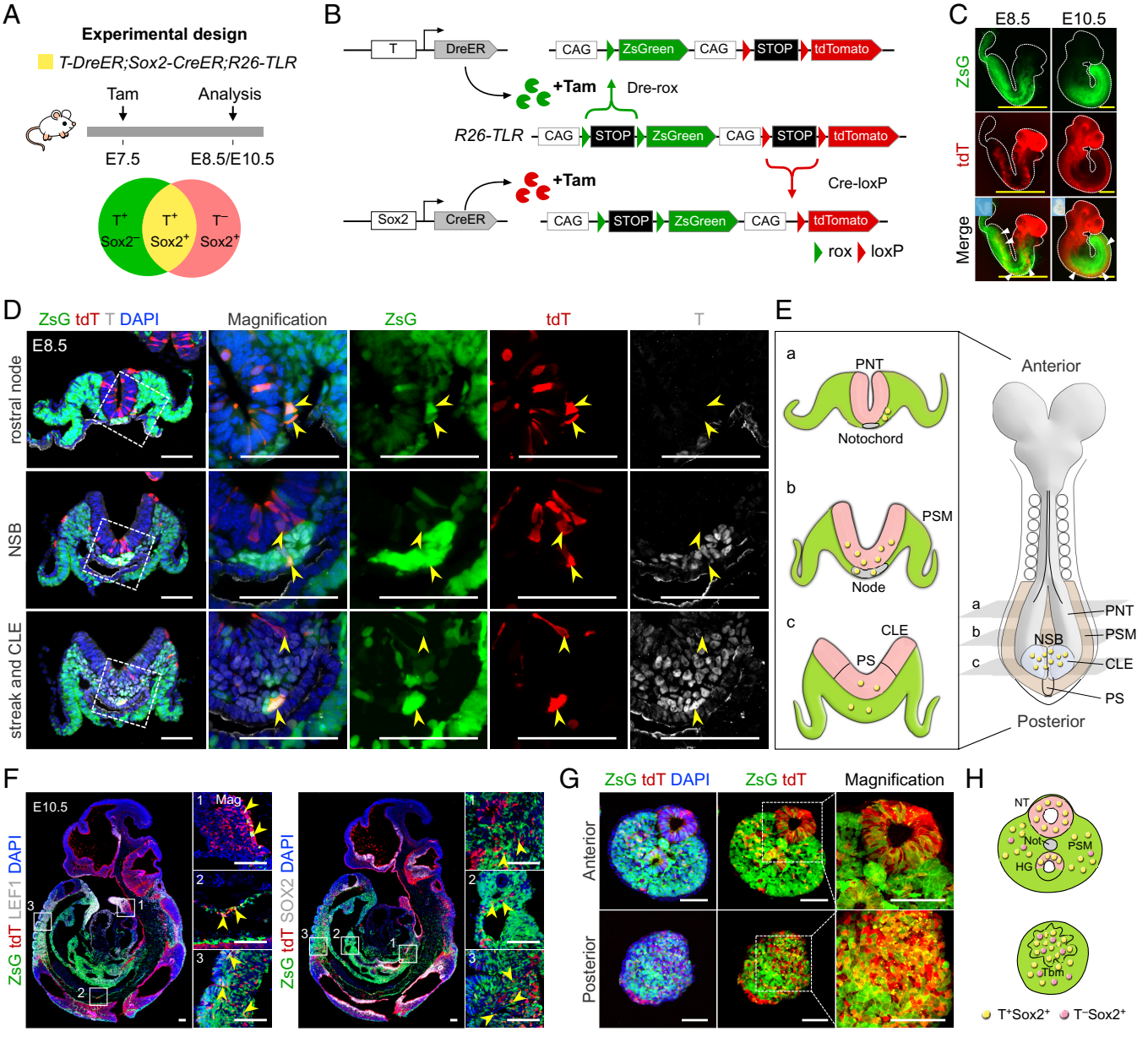

Fig. 2. Lineage tracing of NMPs by *T-DreER;Sox2-CreER;R26-TLR*. (*A*) Schematic figure showing the experimental design. The lower panel illustrates the intersectional genetic labeling of T^+ cells (ZsG^+), $Sox2^+$ cells (tdT^+), and T^+Sox2^+ cells (ZsG^+tdT^+) by *T-DreER;Sox2-CreER;R26-TLR* mice. (*B*) Schematic showing the results after Dre-*rox* or Cre-*loxP* recombination. (*C*) Whole-mount bright-field and epifluorescence imaging of E8.5 and E10.5 *T-DreER;Sox2-CreER;R26-TLR* embryos. (*D*) Immunostaining for ZsG, tdT, and T on tissue sections collected from E8.5 *T-DreER;Sox2-CreER;R26-TLR* embryos. (*E*) Cartoon showing the distribution of NMPs at E8.5. Green, T^+ cells; red, $Sox2^+$ cells; yellow, T^+Sox2^+ cells. PNT, preneural tube; PSM; PS, primitive streak; CLE; NSB. (*F*) Immunostaining for ZsG, tdT, LEF1, or SOX2 on tissue sections collected from E10.5 embryos. Arrowheads indicate T^+Sox2^+ cells. (*G*) Immunostaining for ZsG and tdT on E10.5 tail bud tissue sections. (*H*) Cartoon showing the distribution of NMPs in E10.5 tail bud. Green, T^+ cells; red, $Sox2^+$ cells; yellow, T^+Sox2^+ cells. NT, neural tube; Not, notochord; PSM; HG, hindgut; Tbm, tail bud mesenchyme. (Scale bars: yellow, 1 mm; white, 100 μm.)

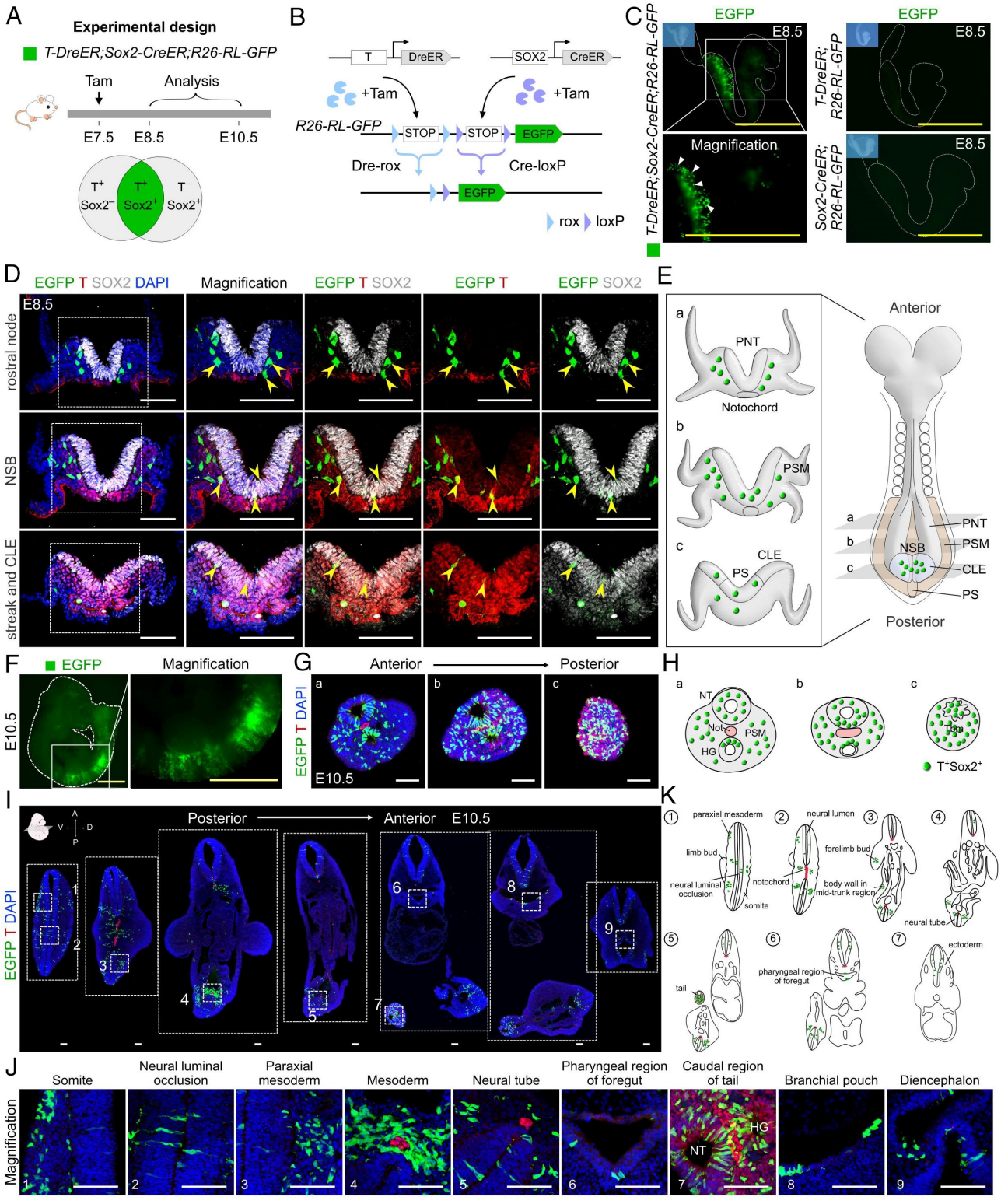

Fig. 3. Lineage tracing of NMPs by *T-DreER;Sox2-CreER;R26-RL-GFP*. (*A*) Schematic showing the experimental design and the strategy for labeling T^+Sox2^+ cells ($EGFP^+$) by *T-DreER;Sox2-CreER;R26-RL-GFP* mice. (*B*) Schematic diagram showing the genetic approach for labeling T^+Sox2^+ cells. (*C*) Whole-mount bright-field and epifluorescence images of E8.5 embryos of the indicated genotype after Tam treatment. (*D*) Immunostaining for EGFP, T, and SOX2 on tissue sections collected from E8.5 embryos. Arrowheads indicate T^+Sox2^+ cells. (*E*) Cartoon showing the distribution of NMPs at E8.5 by *T-DreER;Sox2-CreER;R26-RL-GFP* genetic tool. Green, T^+Sox2^+ cells. PNT, preneural tube; PSM; PS, primitive streak; CLE; NSB. (*F*) Whole-mount bright-field and epifluorescence images of E10.5 embryos of *T-DreER;Sox2-CreER;R26-RL-GFP*. (*G*) Immunostaining for EGFP and T on serial embryonic sections collected from E10.5 embryonic tail bud. (*H*) Cartoon showing the distribution of NMPs in E10.5 tail bud. Green, T^+Sox2^+ cells. NT, neural tube; Not, notochord; PSM; HG, hindgut; Tbm, tail bud mesenchyme. (*I* and *J*) Immunostaining for EGFP and T on serial E10.5 embryonic sections from posterior to anterior. Panel *J* shows the magnified images from the white dotted boxes in panel *I*. (*K*) Cartoon showing the distribution of NMPs in E10.5 whole embryo by *T-DreER;Sox2-CreER;R26-RL-GFP* mice. Green, T^+Sox2^+ cells; red, T antibody positive cells. (Scale bars: yellow, 1 mm; white, 100 μm.)

were found in all three germ layers but were restricted to the posterior region of the embryos at E8.5 (*SI Appendix*, Fig. S3 *F* and *G*). These cells exhibited an expression pattern similar to that of the transgenic mouse line *TCreERT2* (7). Further analysis of the traced E10.5 embryos revealed that the labeled ZsGreen$^+$ cells contributed not only to the majority of the mesodermal descendants but also to the neural tube, hindgut, and pharyngeal region of the foregut (*SI Appendix*, Fig. S3 *H* and *I*). Moreover, no ZsGreen$^+$ cells were detected in the *T-DreER;R26-TLR* embryos without Tam administration, and the absence of tdT-expressing cells indicated that there was no leaky expression or cross-talk in this intersectional genetic system (*SI Appendix*, Fig. S3 *E–G*). We then crossed the *Sox2-CreER* knock-in mouse with the *R26-TLR* reporter and induced Cre-*loxP* recombination at E7.5 (*SI Appendix*, Fig. S3 *J–L*). Whole-mount epifluorescence imaging and immunostaining results demonstrated that neural cells were efficiently labeled as tdT$^+$ cells, while no ZsGreen$^+$ cells were found in the *Sox2-CreER;R26-TLR* embryos (*SI Appendix*, Fig. S3 *N–Q*). Additionally, no tdT signal was detected without Tam (*SI Appendix*, Fig. S3*M*). Collectively, these data indicate that the populations of cells expressing *T* and *Sox2* can be effectively labeled by the *T-DreER* and *Sox2-CreER* mouse lines, respectively.

After characterizing the *T-DreER* and *Sox2-CreER* mice, we generated *T-DreER;Sox2-CreER;R26-TLR* mice to specifically label T$^+$Sox2$^+$ NMPs. With this genetic tool, we aimed to delineate the spatiotemporal distribution of NMPs during late developmental stages. We first administered a single dose of Tam to pregnant mice at E6.5 and analyzed them at E7.5 (*SI Appendix*, Fig. S4*A*). As shown in *SI Appendix*, Figs. S4 *B* and *C*, ZsGreen$^+$tdT$^+$ cells were found in the posterior region of the epiblast, suggesting that NMPs originate from the primitive streak in the developing embryos (*SI Appendix*, Fig. S4 *B* and *C*). Next, we injected Tam at E7.5 and collected embryos at E8.5 (Fig. 2*A*). Whole-mount fluorescent imaging of embryos showed that cells in the caudal region prominently expressed ZsGreen, while those in the headfold region mainly expressed tdT (Fig. 2*C*). Immunostaining for ZsGreen, tdT, and T/SOX2 in serial sections of E8.5 embryos demonstrated that ZsGreen$^+$tdT$^+$ cells were predominantly located within the epiblast of the NSB and posteriorly within the CLE and primitive streak (Fig. 2 *D* and *E*). Lineage tracing of NMPs at E10.5 showed that ZsGreen$^+$tdT$^+$ cells were largely confined to the caudal domain of the embryo, contributing to the neural tube and adjacent paraxial mesoderm, but not to the notochord (Fig. 2*F* and *SI Appendix*, Fig. S4 *D* and *E*). Specifically, in the tail region, ZsGreen$^+$tdT$^+$ cells were detected in the newly formed neural tube and posteriorly in the contiguous tail bud mesenchyme (Fig. 2 *G* and *H*). To our surprise, a small number of ZsGreen$^+$tdT$^+$ cells were also found in the pharyngeal region of the foregut, indicating that T$^+$Sox2$^+$ cells may potentially contribute to the endoderm (Fig. 2*F*). Taken together, these findings indicate that double-positive cells were primarily localized within the mouse NSB and CLE at E8.5 and in the tail bud region at E10.5, largely contributing to the formation and elongation of the caudal neural tube and adjacent paraxial mesoderm.

Generation of an Intersectional Genetic Approach for Specific Targeting NMPs. To specifically trace NMPs during body axis elongation, we developed a second intersectional genetic approach by generating the *T-DreER;Sox2-CreER;R26-RL-GFP* mouse. This involved crossing *T-DreER* and *Sox2-CreER* mice with the dual recombinase–responsive *R26-RL-GFP* reporter mice (36). In this system, GFP activation required both Dre-*rox* and Cre-*loxP* recombination to remove two *Stop* cassettes. Consequently, only the T$^+$Sox2$^+$ cells could be genetically labeled with GFP, while single-positive cell populations, such as T$^+$Sox2$^-$ or T$^-$Sox2$^+$ cells, remained unlabeled (Fig. 3 *A* and *B*). As a technical control, no GFP$^+$ cells were detected in E10.5 embryos without Tam treatment, confirming the absence of leakiness in the *R26-RL-GFP* system (*SI Appendix*, Fig. S5 *A–C*). Whole-mount fluorescence imaging and immunostaining of *T-DreER;R26-RL-GFP* or *Sox2-CreER;R26-RL-GFP* embryos showed no GFP$^+$ cells throughout the entire embryo after Tam administration, demonstrating that there was no cross-talk between the dual recombinases (Fig. 3*C* and *SI Appendix*, Figs. S5 *D–F*). These data demonstrate that *R26-RL-GFP* is specific for tracing double-positive cells in vivo.

We next collected *T-DreER;Sox2-CreER;R26-RL-GFP* embryos for analysis at E8.5 and E10.5 after Tam induction at E7.5 (Fig. 3*A*). Whole-mount fluorescence images showed that the labeled GFP$^+$ cells were primarily restricted to the caudal region of the embryos (Fig. 3 *C*, *Left*, and *F*). Immunostaining for GFP, T, and SOX2 in serial sections of E8.5 embryos demonstrated that the NMPs labeled with *T-DreER;Sox2-CreER;R26-RL-GFP* were predominantly located in the epiblast layer of the NSB and CLE (Fig. 3 *D* and *E*). Lineage tracing of T$^+$Sox2$^+$ NMPs in the tails of E10.5 embryos revealed that GFP$^+$ cells mainly contributed to the neural tube, paraxial mesoderm, and hindgut, but not to the notochord. Posteriorly, GFP$^+$ cells were also found in the tail bud mesenchyme (Fig. 3 *G* and *H*). In whole embryos, GFP$^+$ cells were primarily located in the somites, neural luminal occlusion, paraxial mesoderm, neural tube, and the caudal region of the tail. Consistent with the results from the *R26-TLR* genetic tracing system, labeled GFP$^+$ cells were detected in some endoderm-derived tissues, such as the pharyngeal region of the foregut and the branchial pouch (Fig. 3 *F* and *I–K*). Furthermore, after Tam treatment at E7.5, the labeled GFP$^+$ cells were largely concentrated in the trunk and tail regions, with their descendants contributing minimally to other tissues by E14.5 (*SI Appendix*, Fig. S6 *A– C*). Notably, when Tam was induced at E10.5 or E11.5, the labeled T$^+$Sox2$^+$ cells were strongly restricted to the tip region of the tail and were rarely detected in other regions (*SI Appendix*, Fig. S6 *D–I*).

Taken together, the above data suggest that NMPs contribute to multiple organ systems derived from the mesoderm, ectoderm, and endoderm during development. The different dual genetic tracing systems developed in this study clearly delineate the in vivo fate map of NMPs and their immediate descendants throughout body axis elongation.

Lineage Tracing Reveals the Bipotency of NMPs During Axis Elongation. Previous clonal studies have suggested that common progenitors are responsible for the development of neural tube and mesodermal cells at a population level (2, 21, 37). However, the differentiation potential of a single NMP cell remains unclear. Our sequencing data from E8.5, particularly the RNA velocity analysis, indicate that neural and somatic developmental trajectories arise from NMPs (Fig. 4*A*). The pseudotime derived from RNA velocity accurately reconstructed the internal clock of the cells, revealing that NMPs were produced earlier than those in the PSM and neural tube (Fig. 4*B*). The pseudotemporal trajectory illustrated that the ordering of CLE-derived cells showed a genetic cascade from NMPs to neural or mesodermal progenitors, highlighting an in vivo spatiotemporal differentiation pathway (Fig. 4*C*). To directly investigate the differentiation potential of individual NMPs, we employed the dual recombinase–responding *R26-confetti2* reporter mice (38, 39) for single-cell clonal analysis to determine the cell fate of individual NMPs. Unlike the conventional *R26-Confetti* reporter, which responds only to Cre, the *R26-confetti2* reporter displayed unique fluorescent signals after both Dre-mediated and Cre-mediated recombination.

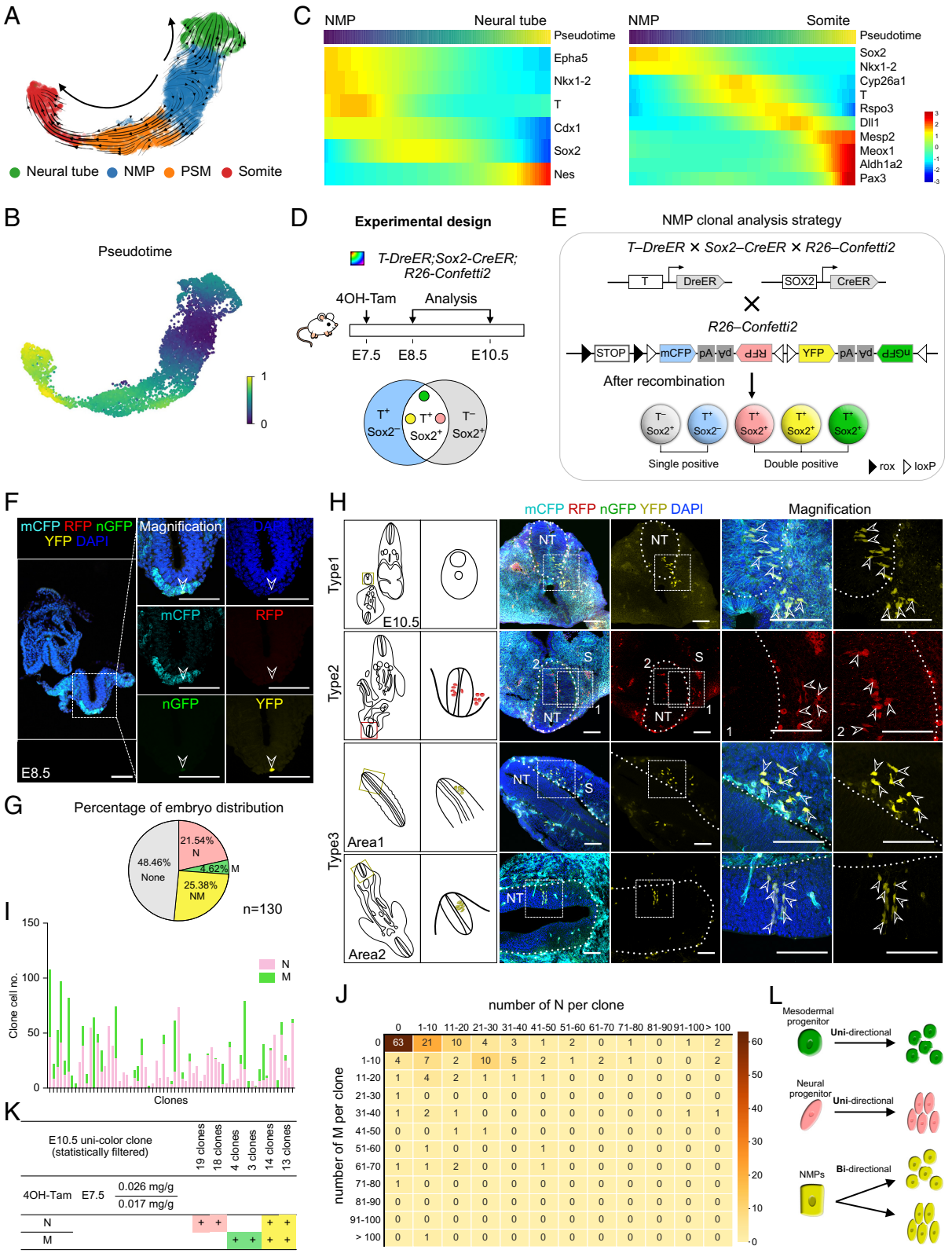

Fig. 4. Bidirectional potency of single NMP during embryo development. (*A*) UMAP colored by identified clusters with trajectories inferred from RNA velocity. (*B*) Pseudotime based on RNA velocity showing that NMPs are produced earlier than PSM and neural tube along the trajectory. (*C*) Heatmap with scaled expression of genes involved in neural development (*Left*) or somitogenesis (*Right*) from E8.5 caudal region and ordered by pseudotime. (*D*) Schematic showing the experimental design and distinct cell labeling after Cre or Dre recombination. (*E*) Schematic showing strategy for labeling of single NMPs. (*F*) Fluorescent image of E8.5 embryonic section of *T-DreER;Sox2-CreER;R26-Confetti2*. (*G*) Cartoon and fluorescent images illustrating the different bidirectional clonal formation types of single NMP in E10.5 embryos. Boxed regions are magnified. (*H*) The pie chart showing the percentage of embryo number with no clone, unidirectional clone, or bidirectional clone from 130 *T-DreER;Sox2-CreER;R26-Confetti2* embryos collected at E10.5. (*I*) A chart showing the cell number of neural and mesodermal cells in each clone. (*J*) The matrix indicates the relative frequency of certain clone composition, with deeper shading indicating higher frequency. N in the *x* axis; M in the *y* axis. (*K*) Clonal analyses of unicolor E10.5 embryos reveal that individual clone labeled at E7.5 has the capacity to generate neural and mesodermal cells within the embryos. (*L*) Cartoon showing that single NMP expands to three types of clones during embryo development. N, neural cells; M, mesodermal cells; NM, neuromesodermal cells. (Scale bars, white, 100 μm.)

In this design, *T-DreER*, *Sox2-CreER*, and *Rosa26-Confetti2* mice were crossed to generate *T-DreER;Sox2-CreER;Rosa26-Confetti2* embryos, enabling the labeling of individual NMPs with distinct colors. A single low dose of Tam was administered at E7.5 to facilitate sparse labeling of cells, and embryos were harvested at E8.5 and E10.5 to assess the cell fate commitment of individual NMPs (Fig. 4*D*). Following Dre-*rox* and Cre-*loxP* recombinations, the double-positive NMPs (T^+Sox2^+) were stochastically labeled as one of three fluorescent proteins (RFP, YFP, or GFP), while the single-positive T^+ and $Sox2^+$ cells were labeled as CFP or remained unlabeled, respectively (Fig. 4 *D* and *E*). In our experiments, an appropriate dosage of 4OH-Tam was administrated at E7.5 to ensure that only single-color cells were labeled at E8.5. Given the characteristics of 4OH-Tam, we inferred that cells observed at subsequent developmental stages with the same color were likely derived from the original labeled single cell at E8.5. Serial fluorescent imaging of E8.5 *T-DreER;Sox2-CreER;Rosa26-Confetti2* embryonic sections revealed that the embryos contained only YFP-labeled clones (Fig. 4*F*). To ensure that the labeling efficiency was sufficiently low to allow only single-cell labeling, nearly half of the 130 *T-DreER;Sox2-CreER;Rosa26-Confetti2* embryos were observed to lack a labeled cell at E10.5 (Fig. 4*G*). Considering this sparse single-cell labeling condition, we next analyzed the clonal expansion and cell fate commitment of the labeled NMPs.

Serial fluorescent imaging of E10.5 embryos from anterior to posterior revealed three distinct clones based on their cell fates: neural, mesodermal, and mixed clones containing both neural and mesodermal cells. In the mixed clones, cells displayed three different clonal positions: Type 1, neural and mesodermal cells of the same clone aligned continuously across the neural tube border; Type 2, neural and mesodermal cells of the same clone were noncontinuously aligned within the same tissue section, indicating that the labeled single-color cell expanded and distributed to both neural and mesodermal tissues, maintaining a certain spatial distance on the slice; and Type 3, neural and mesodermal cells of the same clone localized in separate niches across different tissue sections (Fig. 4*H*). Moreover, we quantified the number of cells in each clone contributing to different lineages and found that there were more neural clones than mesodermal ones at E10.5 (Fig. 4*I* and *J*). Nevertheless, there was no significant difference in clone numbers between neural and mesodermal clones at E12.5 and E14.5. It is noteworthy that the number of mesodermal cells in each clone increased, leading to a more dominant population over time (*SI Appendix*, Fig. S7*A*).

To reduce the likelihood of observing multirecombinant clones, we included only those with a single fluorescent signal (i.e., RFP, YFP, or GFP) that passed a statistical filter based on the Gaussian mixture model for further analysis. The quantification results supported the bipotency of individual NMPs, as demonstrated by varying doses of 4OH-Tam (Fig. 4*K*). Moreover, we reanalyzed the clones to examine whether individual NMPs could differentiate into neural, mesodermal, and endodermal lineages. We found that 10 out of 176 clones could differentiate into endodermal cells, but this proportion was relatively small. After filtering, further analysis showed that only a small subset of the labeled T^+Sox2^+ cells could differentiate into the endodermal lineage (*SI Appendix*, Fig. S7 *B*–*D*). Overall, our dual recombinase–mediated single-cell clonal analysis revealed that individual NMPs are bipotent and can contribute to both neural and paraxial mesodermal lineages during vertebrate body elongation (Fig. 4*L*).

Specific Ablation of NMPs Results in Malformed Embryonic Trunks and Tails. The data presented above demonstrate the contribution of NMPs to the development of the spinal cord and paraxial mesoderm. To directly determine the potential function of these NMPs during embryonic development, we generated *T-DreER;Sox2-CreER;R26-LR-DTR* mice to deplete NMPs through dual recombinase–mediated expression of the diphtheria toxin receptor (DTR), followed by treatment with diphtheria toxin (DT) treatment (40) (Fig. 5 *A* and *B*). To ensure efficient delivery of DT into the embryos, we injected it directly into the developing embryos, as described in Fig. 5*C* (41). Compared to those treated with PBS, the body and tail lengths of wild-type embryos injected with DT at E9.5 were grossly normal, showing no significant difference at E14.5 (*SI Appendix*, Fig. S8). Thus, the adverse effects of DT during embryonic development were excluded from our data interpretation.

Next, we injected DT into E9.5 embryos that had been treated with Tam at E7.5 and collected *T-DreER;Sox2-CreER;R26-LR-DTR* and littermate control embryos for analysis at E14.5. Approximately 20% of these embryos exhibited abnormal trunk and tail development (Fig. 5*D*). Some embryos displayed normal development after NMP ablation, which may be attributed to low absorption efficiency of DT, or to compensation by surrounding cells for the loss of NMPs in some embryos. Whole-mount bright-field imaging and quantification analysis indicated that the NMP-depleted embryos had a normal body length but a notably shorter tail at E14.5 (Fig. 5 *E* and *F*). Immunostaining for SOX2 and LEF1 in embryonic sections revealed a profound reduction in $SOX2^+$ and $LEF1^+$ cells in the trunks and tails of NMPs-ablated embryos (Fig. 5*G*). Furthermore, histological analysis showed malformed trunks and tails in the embryos after NMP depletion (Fig. 5*H*).

To further explore the roles of NMPs at different time points, we injected *T-DreER;Sox2-CreER;R26-LR-DTR* embryos with DT at E8.5 or E10.5 (*SI Appendix*, Fig. S9*A*). Compared to control embryos that did not receive DT, the NMP-depleted embryos showed unaffected body length but slightly reduced tail length at E14.5 when DT was administered at E8.5 (*SI Appendix*, Fig. S9 *B* and *C*). These minor defects may result from inadequate NMP deletion at E8.5 or compensation from other cell lineages. In contrast, after NMP ablation at E10.5, the embryos exhibited severely undeveloped trunks and tails (*SI Appendix*, Fig. S9 *B* and *C*). Immunostaining for SOX2 and LEF1 in embryonic sections further showed a reduction in $SOX2^+$ and $LEF1^+$ cells after DT treatment at either E8.5 or E10.5 (*SI Appendix*, Fig. S9*D*).

To investigate the small effects observed when DT was administrated at E8.5, we collected NMP-depleted *T-DreER;Sox2-CreER;R26-LR-DTR/RL-GFP* embryos and control *T-DreER;Sox2-CreER;R26-RL-GFP* embryos at E9.5 and E10.5, respectively, following Tam treatment at E7.5 (*SI Appendix*, Fig. S10*A*). Whole-mount fluorescent imaging showed a significant decrease in GFP signals in the NMP-depleted embryos (*SI Appendix*, Fig. S10*B*). Immunostaining for GFP in tail sections, along with quantification analysis of the percentage of GFP^+ cells in DAPI-stained sections, further revealed a significant reduction in GFP^+ cells in NMP-depleted embryos (*SI Appendix*, Fig. S10 *C* and *D*). These results demonstrate that the minor phenotypes observed in *T-DreER;Sox2-CreER;R26-LR-DTR* embryos at later developmental stages were likely due to compensatory effects from adjacent cell populations.

To ascertain whether single positive cells could compensate for the loss of double positive cells, we collected NMP-depleted *T-DreER;Sox2-CreER;R26-LR-DTR/TLR* embryos and control *T-DreER;Sox2-CreER;R26-TLR* embryos at E14.5, following DT administration at E9.5 (*SI Appendix*, Fig. S11*A*). As shown in *SI Appendix*, Fig. S11*B*, compared to the controls, the single T^+ (ZsG^+) cells appeared to increase in the tail region of the less severely NMP-depleted embryos, while the $Sox2^+$ (tdT^+) cells

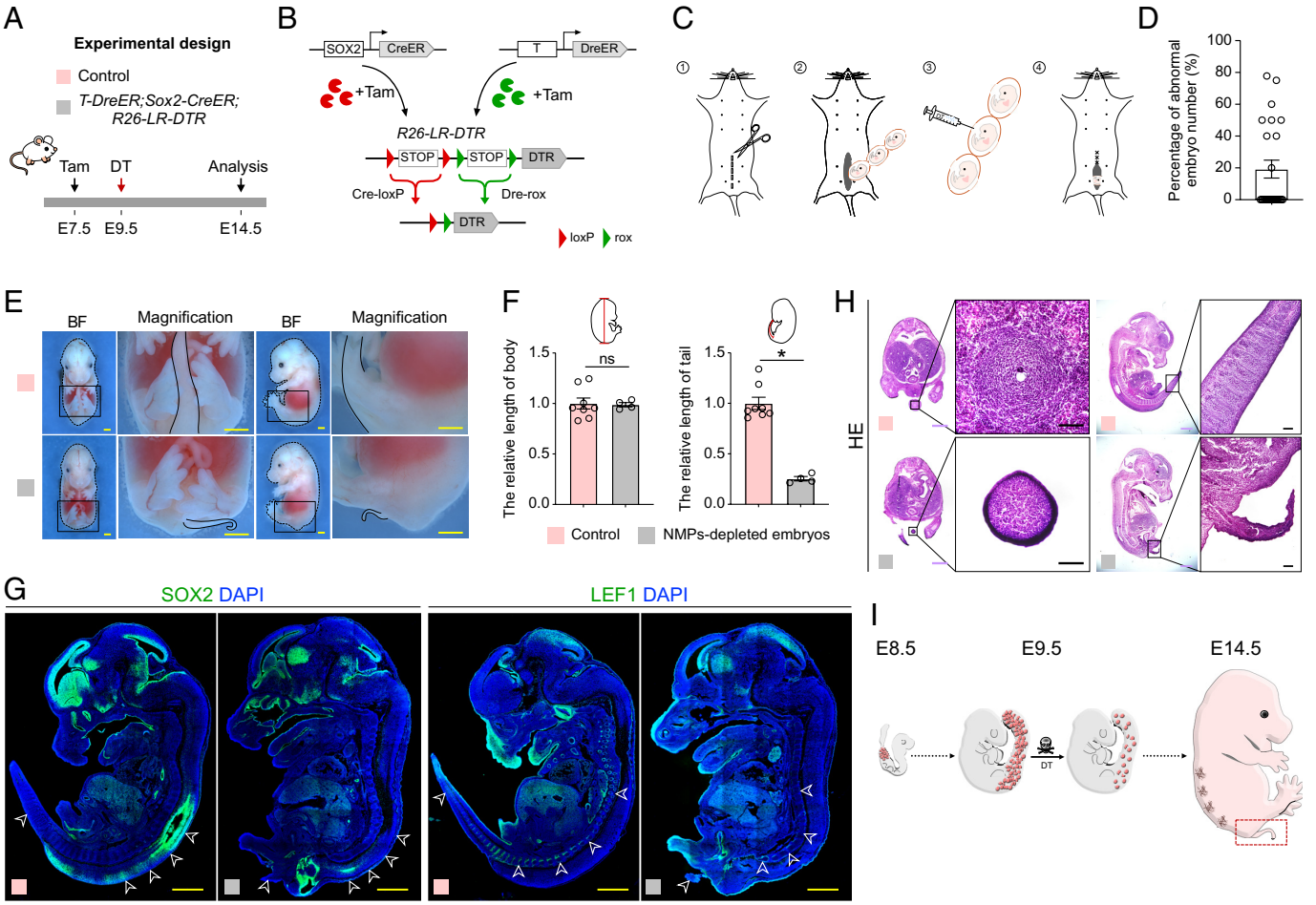

Fig. 5. Genetic ablation of NMPs leads to defective trunk and tail growth. (*A*) Schematic showing the experimental design. (*B*) Schematic showing NMP depletion strategy by DTR expression after Cre-*loxP* and Dre-*rox* recombination. (*C*) Scheme illustrating the process of DT injection at the embryonic stage. (*D*) Quantification of the percentage of abnormal embryos of *T-DreER;Sox2-CreER;R26-LR-DTR* after DT treatment. Data are the mean ± SEM; n = 24 mice per group. (*E*) Whole-mount bright-field images of embryos at E14.5 after DT treatment between littermate controls (*T-DreER;R26-LR-DTR*, *Sox2-CreER;R26-LR-DTR*, or *R26-LR-DTR*) and NMP-depleted groups (*T-DreER;Sox2-CreER;R26-LR-DTR*). (*F*) Quantification of the relative body length and tail length after DT treatment between littermate controls and NMP-depleted groups. For NMP-depleted groups, only embryos with short tails were included. Data are the mean ± SEM; n ≥ 4 mice per group; ns nonsignificant. (*G*) Immunostaining for SOX2 (*Left*) and LEF1 (*Right*) on controls and NMP-depleted groups at E14.5. (*H*) H&E staining of E14.5 embryonic sections after DT treatment. (*I*) Cartoon showing that ablation of NMPs leads to defective trunk and tail development. (Scale bars: yellow, 1 mm; purple, 1 mm; black, 100 μm; white, 100 μm.)

showed no significant change. In the more severely NMP-depleted embryos, we observed a significant increase in single T^+ (ZsG^+) cells in the shortened tail (*SI Appendix*, Fig. S11*B*). These findings suggest that the ablation of T^+Sox2^+ cells led to an increase in single T^+ cells in the tail region. In addition, immunostaining for endoderm marker genes FOXA2 and SOX17 in E14.5 embryonic sections demonstrated no significant differences in expression levels of these markers between control embryos and severely NMP-depleted embryos (*SI Appendix*, Fig. S11 *C* and *D*). Furthermore, histological analysis revealed normal structures of gut endoderm-derived tissues after NMP depletion, indicating that the gut endoderm remained unaffected by the loss of NMPs (*SI Appendix*, Fig. S11*E*).

Although the current study primarily focuses on the contribution of T^+Sox2^+ NMPs to somitogenesis, our results also suggest the potential involvement of other progenitor cells in this developmental process. Previous research has reported that lower or absent expression of T can prolong the maintenance of the self-renewing progenitor pool in the streak region, ensuring complete axial elongation (42). More recently, scRNA-seq has demonstrated that $T^{-/-}$ cells still contribute to posterior somitic tissues, highlighting their role even in the absence of T (43). T-independent regulators ingress through the primitive streak before E7.0, and the contribution of $T^{-/-}$ cells to the posterior somitic mesoderm was evidenced in E8.5 chimeras. This suggests that early progenitors may still contribute to the developing pool of NMPs, even when T expression is lacking. Our observations align with these findings, as we noted milder segmentation defects after DT injection at E8.5. At this stage, early precursors in the streak region could still contribute to the development of NMPs later on. In contrast, a more severe phenotype characterized by reduction in body length and tail formation was observed after DT injection at E10.5, when those precursors had already differentiated into NMPs that were subsequently depleted. Furthermore, the stochastic expression of segmentation clock genes, influenced by environmental stressors such as temperature and hypoxia, can also trigger variable somite segmentation phenotypes, even among genetically identical embryos (44). This highlights the need for further investigations into the gene–environmental interactions that regulate NMP development. In summary, our results indicate that NMPs are essential for maintaining the normal structure of the trunk and tail (Fig. 5*I*).

Discussion

In this study, we developed various intersectional genetic methods to specifically target NMPs in vivo, allowing us to delineate their distribution, differentiation potential, and functions during

embryonic development. By integrating scRNA-seq with dual recombinase–mediated genetic lineage tracing, we specifically and efficiently labeled NMPs. Our results showed that NMPs were predominantly localized in the NSB and CLE at E8.5, from which they subsequently contributed to the formation of various neural and mesodermal tissues in later stages of embryonic development. Additionally, single-cell labeled clonal analysis demonstrated the bipotency of NMPs during mouse axis elongation, underscoring their versatile differentiation capabilities. The genetic ablation of NMPs resulted in severely abnormal and underdeveloped tails in a subset of the mice, highlighting the critical role of these progenitor cells in proper trunk and tail formation. Collectively, our results provide direct genetic evidence that enhances our understandings of cell fate commitment and the functional roles of NMPs during embryonic development. Moreover, these insights may pave the way for identifying cellular targets in the study of somitogenesis and could reveal the therapeutic potential of NMPs in regenerative medicine.

NMPs play a crucial role in the development of both neural and mesodermal tissues along the anterior–posterior axis of the developing embryo. Initially located in the CLE, these cells migrate cranially during axis elongation. In 2014, Guillot et al. (9) confirmed the dual-fated potential of in vitro-generated NMPs, and subsequently, Tsakiridis and Wislon (4) reported that individual T^+Sox2^+ cells could generate both neural and mesodermal clones in vitro. These findings have important implications for understanding the stemness of NMPs in vivo. By utilizing lineage tracing and scRNA-seq, Guillot et al. further identified the bipotential fate of NMPs, demonstrating their contribution to both neural and mesodermal lineages in the trunks and tails of chicken embryos (45). Consistent with these findings, our study employed a dual recombinase–mediated clonal analysis strategy that enabled us to specifically label NMPs in vivo at a single-cell resolution within a defined time window. These results, along with functional data, further our understanding of the stemness and functions of NMPs during embryonic development. Importantly, unidirectional NMPs are considered transient progenitors rather than long-term stem cells. They exhibit limited self-renewal capabilities and are characterized by the production of neural and paraxial mesoderm lineages, contributing to the development of the central nervous system (CNS) and axial skeleton, respectively. In contrast, bipotential NMPs have greater self-renewal potential and can give rise to both neural and mesodermal tissues across multiple generations of cell division (21). Gene profiling analysis indicated that NMPs principally function in anterior/posterior pattern specification, stem cell differentiation, and organ morphogenesis. By using dual-recombinase-mediated genetic lineage tracing tools, our work provides compelling genetic evidence regarding NMP cell fate commitment, lineage specification, and functional roles. This addresses a long-standing question about the formation of the CNS, where anterior and posterior neural tissues are generated independently. Furthermore, our study also revealed that T^+Sox2^+ cells, in addition to their established roles in contributing to neural and mesodermal tissues, also give rise to cells in the pharyngeal endoderm within the mouse embryo. This finding expands the known contributions of NMPs and highlights their versatility in embryonic development.

In summary, our study provides valuable insights into the differentiation and function of NMPs during the early stages of embryonic development. By understanding the molecular mechanisms driving NMP development, we can illuminate potential biomedical applications arising from neuromesodermal research. For instance, the molecular signaling pathways identified in our work could facilitate more efficient differentiation of NMPs from human induced pluripotent stem cells (iPSCs). This advancement could significantly impact disease modeling, drug discovery, and even cell therapy for conditions such as spinal cord injuries and skeletal muscle disorders (46). Altogether, our findings highlight the importance of NMPs as promising candidates for regenerative medicine.

Materials and Methods

All mouse experiments performed in this research were approved by the Institutional Animal Care and Use Committee of the Shanghai Institute of Biochemistry and Cell Biology, Center for Excellence in Molecular Cell Science, Chinese Academy of Science. The methods in this study included bioinformatic analyses of sc-RNA sequencing, genomic PCR, tissue whole-mount fluorescence microscopy, immunofluorescent staining and imaging, clonal analysis, hematoxylin and eosin staining, and DT injections. The detailed description of the material and method utilized in this study is provided in *SI Appendix*.

Data, Materials, and Software Availability. The accession number for the raw sequencing data and processed count matrix reported in this paper is GSE229103 (23). Source data are provided with this paper. All other data are included in the manuscript and/or *SI Appendix*.

ACKNOWLEDGMENTS. We thank Cyagen for mouse generation. We also thank members of the animal facility, cell platform and chemical biology technology platform in Center for Excellence in Molecular Cell Science and the National Center for Protein Science Shanghai for assistance in microscopy. This work was supported by the National Key Research & Development Program of China (2024YFA1803302 and 2023YFA1800700), Chinese Academy of Sciences (CAS) Strategic Priority Research Program (CXDB0990101), the National Natural Science Foundation of China (82088101, 32200661, 32370897, and 32100648), Research Grants Council of Hong Kong Research Fellowship (RFS2223-4S04), Research Funds of Hangzhou Institute for Advanced Study (2022ZZ01015 and 2024HIAS-V005), CAS Project for Young Scientists in Basic Research (YSBR-012), Shanghai Pilot Program for Basic Research – CAS, Shanghai Branch (JCYJ-SHFY-2021-0), CAS-Croucher Funding Scheme for Joint Laboratories, New Cornerstone Science Foundation, and the Xplorer Prize.

Author affiliations: [a]Chinese Academy of Sciences Center for Excellence in Molecuar Cell Science-Chinese University of Hong kong (CAS CEMCS-CUHK) Joint Laboratories, New Cornerstone Science Laboratory, State Key Laboratory of Cell Biology, Shanghai Institute of Biochemistry and Cell Biology, Center for Excellence in Molecular Cell Science, Chinese Academy of Sciences, University of Chinese Academy of Sciences, Shanghai 200031, China; [b]Key Laboratory of Systems Health Science of Zhejiang Province, School of Life Science, Hangzhou Institute for Advanced Study, University of Chinese Academy of Sciences, Hangzhou 310024, China; [c]School of Life Science and Technology, ShanghaiTech University, Shanghai 201210, China; and [d]CAS CEMCS-CUHK Joint Laboratories, Department of Chemical Pathology, and Li Ka Shing Institute of Health Sciences, Prince of Wales Hospital, The Chinese University of Hong Kong, Hong Kong 999077, China

1. P. P. Tam, R. R. Behringer, Mouse gastrulation: The formation of a mammalian body plan. *Mech Dev.* **68**, 3–25 (1997).
2. N. Cambray, V. Wilson, Two distinct sources for a population of maturing axial progenitors. *Development* **134**, 2829–2840 (2007).
3. N. Cambray, V. Wilson, Axial progenitors with extensive potency are localised to the mouse chordoneural hinge. *Development* **129**, 4855–4866 (2002).
4. A. Tsakiridis, V. Wilson, Assessing the bipotency of in vitro-derived neuromesodermal progenitors. *F1000Res* **4**, 100 (2015).
5. A. Rodrigo Albors, P. A. Halley, K. G. Storey, Lineage tracing of axial progenitors using Nkx1-2CreER(T2) mice defines their trunk and tail contributions. *Development* **145**, dev164319 (2018).
6. D. Henrique, E. Abranches, L. Verrier, K. G. Storey, Neuromesodermal progenitors and the making of the spinal cord. *Development* **142**, 2864–2875 (2015).
7. R. J. Garriock *et al.*, Lineage tracing of neuromesodermal progenitors reveals novel Wnt-dependent roles in trunk progenitor cell maintenance and differentiation. *Development* **142**, 1628–1638 (2015).
8. F. Koch *et al.*, Antagonistic activities of Sox2 and brachyury control the fate choice of neuro-mesodermal progenitors. *Dev. Cell* **42**, 514–526.e517 (2017).
9. M. Gouti *et al.*, In vitro generation of neuromesodermal progenitors reveals distinct roles for wnt signalling in the specification of spinal cord and paraxial mesoderm identity. *PLoS Biol.* **12**, e1001937 (2014).

10. S. Edri, P. Hayward, W. Jawaid, A. Martinez Arias, Neuro-mesodermal progenitors (NMPs): A comparative study between pluripotent stem cells and embryo-derived populations. *Development* **146**, dev180190 (2019).
11. A. Tsakiridis *et al.*, Distinct Wnt-driven primitive streak-like populations reflect in vivo lineage precursors. *Development* **141**, 1209–1221 (2014).
12. F. J. Wymeersch *et al.*, Position-dependent plasticity of distinct progenitor types in the primitive streak. *eLife* **5**, e10042 (2016).
13. M. Bergsland *et al.*, Sequentially acting Sox transcription factors in neural lineage development. *Genes Dev.* **25**, 2453–2464 (2011).
14. B. L. Martin, D. Kimelman, Canonical Wnt signaling dynamically controls multiple stem cell fate decisions during vertebrate body formation. *Dev. Cell* **22**, 223–232 (2012).
15. V. Wilson, I. Olivera-Martinez, K. G. Storey, Stem cells, signals and vertebrate body axis extension. *Development* **136**, 1591–1604 (2009).
16. M. J. Anderson *et al.*, TCreERT2, a transgenic mouse line for temporal control of Cre-mediated recombination in lineages emerging from the primitive streak or tail bud. *PLoS ONE* **8**, e62479 (2013).
17. V. Wilson, L. Manson, W. C. Skarnes, R. S. P. Beddington, The T-gene is necessary for normal mesodermal morphogenetic cell movements during gastrulation. *Development* **121**, 877–886 (1995).
18. K. Arnold *et al.*, Sox2(+) adult stem and progenitor cells are important for tissue regeneration and survival of mice. *Cell Stem Cell* **9**, 317–329 (2011).
19. A. Di-Gregorio *et al.*, BMP signalling inhibits premature neural differentiation in the mouse embryo. *Development* **134**, 3359–3369 (2007).
20. C. D. Stern *et al.*, Head-tail patterning of the vertebrate embryo: One, two or many unresolved problems?. *Int. J. Dev. Biol* **50**, 3–15 (2006).
21. E. Tzouanacou, A. Wegener, F. J. Wymeersch, V. Wilson, J. F. Nicolas, Redefining the progression of lineage segregations during mammalian embryogenesis by clonal analysis. *Dev. Cell* **17**, 365–376 (2009).
22. J. V. Veenvliet *et al.*, Mouse embryonic stem cells self-organize into trunk-like structures with neural tube and somites. *Science* **370**, eaba4937 (2020).
23. H. Jin *et al.*, Datasets from "Dual genetic tracing demonstrates the heterogeneous differentiation and function of neuromesodermal progenitors in vivo." Gene Expression Omnibus (GEO). http://www.ncbi.nlm.nih.gov/geo/query/acc.cgi?acc=GSE229103. Deposited 13 April 2023.
24. Y. Hao *et al.*, Integrated analysis of multimodal single-cell data. *Cell* **184**, 3573–3587.e3529 (2021).
25. D. A. Turner *et al.*, Wnt/beta-catenin and FGF signalling direct the specification and maintenance of a neuromesodermal axial progenitor in ensembles of mouse embryonic stem cells. *Development* **141**, 4243–4253 (2014).
26. H. Kondoh, T. Takemoto, The origin and regulation of neuromesodermal progenitors (NMPs) in embryos. *Cells* **13**, 549 (2024).
27. R. Sambasivan, B. Steventon, Neuromesodermal progenitors: A basis for robust axial patterning in development and evolution. *Front Cell Dev. Biol.* **8**, 607516 (2020).
28. M. Gouti *et al.*, A gene regulatory network balances neural and mesoderm specification during vertebrate trunk development. *Dev. Cell* **41**, 243–261.e247 (2017).
29. G. Amadei *et al.*, Embryo model completes gastrulation to neurulation and organogenesis. *Nature* **610**, 143–153 (2022).
30. M. Diaz-Cuadros *et al.*, In vitro characterization of the human segmentation clock. *Nature* **580**, 113–118 (2020).
31. A. Aguilera-Castrejon *et al.*, Ex utero mouse embryogenesis from pre-gastrulation to late organogenesis. *Nature* **593**, 119–124 (2021).
32. T. Rito, A. R. G. Libby, M. Demuth, J. Briscoe, Notochord and axial progenitor generation by timely BMP and NODAL inhibition during vertebrate trunk formation. bioRxiv [Preprint] (2023). https://doi.org/10.1101/2023.02.27.530267 (Accessed 27 February 2023).
33. J. Zhai *et al.*, Primate gastrulation and early organogenesis at single-cell resolution. *Nature* **612**, 732–738 (2022).
34. L. He *et al.*, Enhancing the precision of genetic lineage tracing using dual recombinases. *Nat. Med.* **23**, 1488–1498 (2017).
35. K. Liu *et al.*, Triple-cell lineage tracing by a dual reporter on a single allele. *J. Biol. Chem.* **295**, 690–700 (2020).
36. M. Han *et al.*, Dual genetic tracing reveals a unique fibroblast subpopulation modulating cardiac fibrosis. *Nat. Genet.* **55**, 665–678 (2023), 10.1038/s41588-023-01337-7.
37. L. Mathis, J. F. Nicolas, Different clonal dispersion in the rostral and caudal mouse central nervous system. *Development* **127**, 1277–1290 (2000).
38. X. Han *et al.*, Lineage tracing reveals the bipotency of SOX9+ hepatocytes during liver regeneration. *Stem Cell Rep.* **12**, 624–638 (2019).
39. K. Liu *et al.*, Bi-directional differentiation of single bronchioalveolar stem cells during lung repair. *Cell Discov.* **6**, 1 (2020).
40. H. Wang *et al.*, Dual Cre and Dre recombinases mediate synchronized lineage tracing and cell subset ablation in vivo. *J. Biol. Chem.* **298**, 101965 (2022).
41. L. Landsman *et al.*, Pancreatic mesenchyme regulates epithelial organogenesis throughout development. *PLoS Biol.* **9**, e1001143 (2011).
42. V. Wilson, R. Beddington, Expression of T protein in the primitive streak is necessary and sufficient for posterior mesoderm movement and somite differentiation. *Dev. Biol.* **192**, 45–58 (1997).
43. C. Guibentif *et al.*, Diverse routes toward early somites in the mouse embryo. *Dev. Cell* **56**, 141–153. e146 (2021).
44. K. Keseroglu *et al.*, Stochastic gene expression and environmental stressors trigger variable somite segmentation phenotypes. *Nat. Commun.* **14**, 6497 (2023).
45. C. Guillot, Y. Djeffal, A. Michaut, B. Rabe, O. Pourquie, Dynamics of primitive streak regression controls the fate of neuromesodermal progenitors in the chicken embryo. *eLife* **10**, e64819 (2021).
46. K. Kajikawa *et al.*, Cell therapy for spinal cord injury by using human iPSC-derived region-specific neural progenitor cells. *Mol. Brain* **13**, 120 (2020).